Available online at www.sciencedirect.com
SCIENCE DIRECT®
Journal of Power Sources 118 (2003) 150–156
JOURNAL OF POWER SOURCES
www.elsevier.com/locate/jpowsour

Protonic ceramic fuel cells for high-efficiency operation with methane

W. Grover Coors*
Protonetics International Inc., Golden, CO, USA

Abstract

A new class of fuel cells is being developed, based on ceramic electrolyte materials that exhibit high protonic conductivity at elevated temperatures. The protonic ceramic fuel cell (PCFC) is fundamentally different and unique among fuel cell types currently being developed because it relies on conduction of protons through the electrolyte at much higher temperatures than is possible with other proton-conducting fuel cells. Operating at 750 °C, the PCFC is ideal for use with hydrocarbon fuels, such as natural gas. Proton conduction implies that water vapor is produced at the cathode, where it is swept away by air, rather than at the anode (as in a solid oxide fuel cell), where it dilutes the fuel. Since carbon dioxide is the only exhaust gas produced, higher fuel utilization is possible. Ambipolar steam permeation from the cathode to the anode provides the steam for direct reforming of hydrocarbons, so external steam injection is not required. Therefore, high thermodynamic efficiency is achieved and coking is not a problem. All of these features make it possible to construct a fuel cell of unprecedented electrical efficiency when operated on hydrocarbon fuels. The principles of operation and the current status of single-cell testing on methane at Protonetics will be described.
© 2003 Elsevier Science B.V. All rights reserved.

Keywords: Protonic ceramic; Steam permeation; Hydrocarbon reforming

1. Introduction

1.1. Electrical efficiency

Fuel cells have the attractive feature of high intrinsic thermodynamic efficiency, compared to other energy conversion technologies. However, this advantage of fuel cells is diminished unless the devices can simultaneously be made to have high fuel utilization. This is particularly true with hydrocarbon fuels, whether derived from fossil fuels or renewable sources. Overall fuel cell efficiency depends on how well these fuels can be reformed to make hydrogen and carbon dioxide.

The main competition for fuel cells in distributed power generation markets is the utility grid. Even in markets for premium and backup power, or where the utility grid is either not available or unreliable, fuel cells must compete with relatively efficient and low-cost internal and external combustion engines/generators that run on hydrocarbon fuels. In order to replace these technologies, fuel cell systems with much more than 40% electrical efficiency will be required. Some insight into the market requirements for fuel cells may be gained by plotting residential utility grid electricity prices versus the cost of pipeline natural gas. Electricity and gas prices are both very volatile, and vary dramatically from country to country and from region to region. Fig. 1 shows the impact of fuel cell efficiency on net operating cost in the United States, given an installed equipment basis of US$ 1000 per kW. In the United States, many regions—particularly in the northeast—have very expensive electricity (greater than US$ 0.12 per kWh) and moderately expensive natural gas (greater than US$ 10 per Mcf (thousand cubic feet)). However, the national average, represented by about US$ 0.08 per kWh and US$ 8.20 per Mcf, can only be reached with fuel cells having electrical efficiencies greater than 55%. Even still, many regions have very low-cost electricity, that cannot be matched by fuel cells at any reasonable fuel conversion efficiency, primarily in areas where hydroelectric power is plentiful.

PEM fuel cells, with electrical efficiencies between 30 and 45% may be able to compete directly with the utility grids in some regions, but the differential cost of electricity between grid and fuel cells are diminishingly small. Current reforming technology precludes PEM (and phosphoric acid fuel cells) from exceeding about 45% efficiency.

SOFCs with 45–55% efficiency are hampered by poor intrinsic fuel utilization because water vapor is produced at the anode where it dilutes the fuel. (See [2] for a detailed analysis of this issue.) New anodes are being developed that permit direct electrochemical oxidation of hydrocarbons

* Tel.: +1-303-278-3113.
E-mail address: g.coors@protonetics.com (W.G. Coors).

0378-7753/03/$ – see front matter © 2003 Elsevier Science B.V. All rights reserved.
doi:10.1016/S0378-7753(03)00072-7

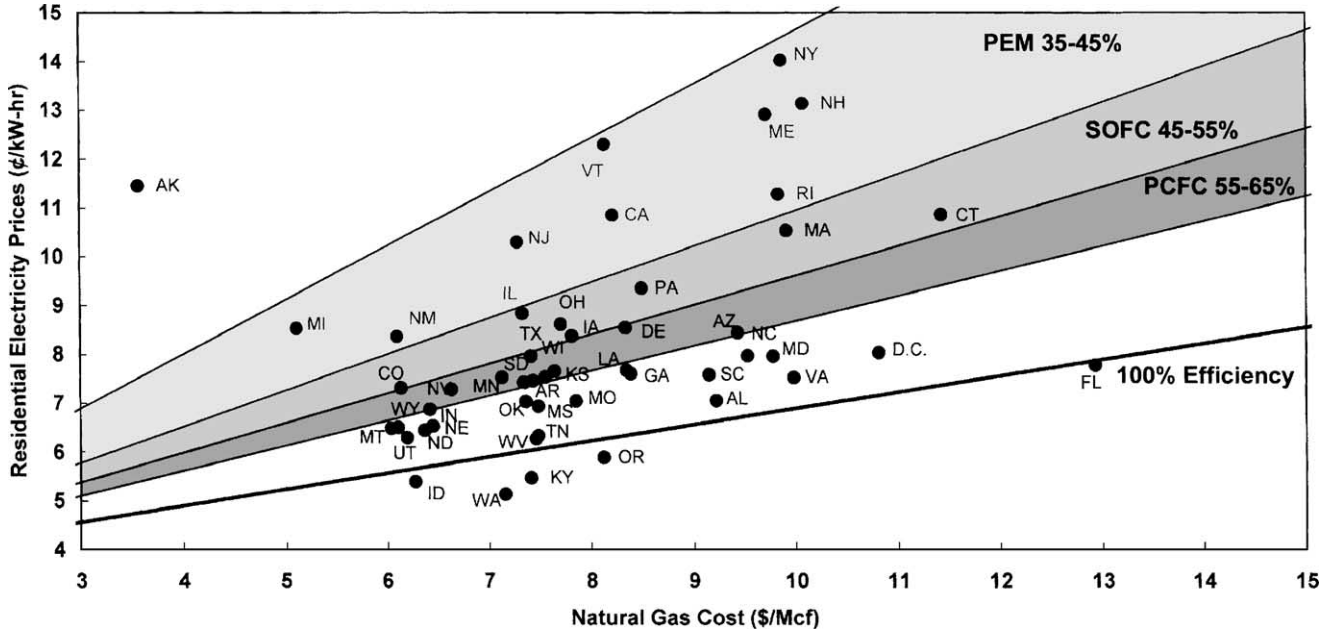

Fig. 1. Residential electricity vs. pipeline natural gas costs in the United States by state [1] US$ 1 per W amortized capital equipment cost of fuel cell system assumed. Assumed electrical efficiency ranges: PEM, 30–45%; SOFC, 45–55%; PCFC, 55–65%.

(e.g. [3]), but even with direct oxidation of methane, two moles of water vapor diluent are introduced into the fuel stream for every mole of methane consumed. Unused fuel in the exhaust stream must either be extracted and returned to the cell or combusted in a subsequent stage. In order to achieve high efficiency, fuel recuperators or gas turbine hybrid operation are required, neither of which are suitable for small-scale, distributed generation. Combined heat and power, CHP, operation [4] has some merit, but commercial viability has yet to be demonstrated for small, distributed systems.

Protonic ceramic fuel cells (PCFCs) are targeted for operation at 55–65% electrical efficiency on pipeline natural gas. This can only be achieved with greater than 90% direct methane fuel utilization. Such high fuel utilization is made possible by three factors. First, high thermochemical efficiency of reforming and water shift reactions at the anode is possible at the high operating temperatures of 700–750 °C. Second, water vapor is produced at the cathode, where it is subsequently swept away by the air flow, rather than at the anode, where it would dilute the fuel (carbon dioxide is the only anode exhaust gas). Third, ambipolar steam permeation through the electrolyte provides the steam required for the reforming and shift reactions, thus preventing hydrocarbon coking and obviating the need for external steam injection.

1.2. Thermochemical analysis

Whereas hydrogen fuel cells realize maximum thermochemical efficiency at low temperatures, direct methane reforming fuel cells require much higher temperatures. Complete oxidation of methane at the anode requires heterogeneous catalysis of the steam reforming and shift reactions, respectively given as

$$CH_4(g) + H_2O_{ads} \rightarrow CO_{ads} + 6H_{ads} \quad (1.1)$$

$$CO_{ads} + H_2O_{ads} \rightarrow CO_2(g) + 2H_{ads} \quad (1.2)$$

Elevated temperatures are needed to promote the very fast reaction kinetics necessary at high current densities in order to reduce activation polarization losses. The ratio of the change in Gibbs energy to the change in enthalpy gives the maximum intrinsic thermochemical efficiency of the methane combustion reaction. This ratio reaches its maximum value at a temperature of about 625 °C, as shown in Fig. 2. (Since the efficiency is greater than 1, it is at least theoretically possible to convert some fuel cell heat into additional electricity.) A fuel cell operating temperature between 600 and 800 °C is, therefore, optimal for direct electrochemical methane conversion.

1.3. Protonic conductivity

A large number of ceramic materials have been identified that can be doped with aliovalent cations to create extrinsic oxygen vacancies. Many of these materials, primarily with the perovskite crystal structure, exhibit the property of high protonic conductivity at moderate temperatures. Water vapor enters the crystal lattice of the ceramic by reacting with one vacant and one occupied oxygen site by the reaction (in Kröger–Vink notation):

$$H_2O(g) + V_0^{\bullet\bullet} + O_0^{\times} \leftrightarrow 2OH_0^{\bullet} \quad (1.3)$$

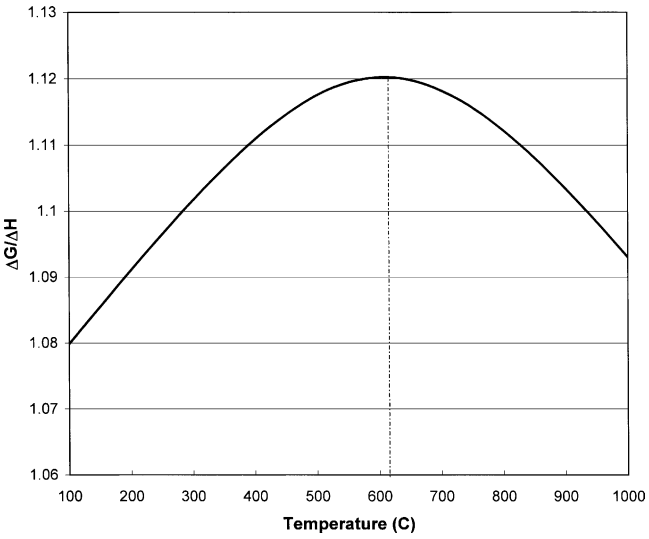

Fig. 2. Thermochemical efficiency ($\Delta G/\Delta H$) of complete combustion of methane as a function of temperature.

producing two protons that are free to hop between oxygen atoms. The concentration and mobility of these protons determine the protonic conductivity of the ceramic. Oxygen vacancies also have significant mobility above 600 °C. Ceramic materials that have large concentrations of oxygen vacancies and for which reaction (1.3) is thermodynamically favorable, become protonated by exposure to water vapor at elevated temperatures. If the protonic conductivity is sufficiently high, typically greater than 10 mS/cm, a useful hydrogen fuel cell may be constructed. Ma et al. [5] identified $BaCe_{0.9}Y_{0.1}O_{3-\alpha}$ (BCY10) as having one of the highest protonic conductivities at 700 °C, with $\sigma = 29$ mS/cm in dry oxygen and $\sigma = 20$ mS/cm in wet hydrogen. These values were obtained by impedance spectroscopy, and are consistent with other researchers working with BCY10 [6]. This electrolyte material has also shown considerable promise in hydrogen concentration cells [7].

Once some fraction of the oxygen vacancies have been filled by protonic defects by reaction (1.3), the electrolyte can sustain a protonic current, where protons are contributed at the anode by the reaction:

$$H_{ads} + O_0^{\times} \rightarrow OH_0^{\bullet} + e' \quad (1.4)$$

and removed at the cathode by the reaction:

$$2OH_0^{\bullet} + \tfrac{1}{2}O_2(g) + 2e' \rightarrow H_2O_{ads} + 2O_0^{\times} \quad (1.5)$$

1.4. Ambipolar steam permeation

Since (1.3) is reversible and does not require electronation or de-electronation at the electrodes, it will proceed independently of reactions (1.4) and (1.5) due to any steam concentration gradient. Ambipolar diffusion is possible without any net current flow in the electrolyte, because the protons and oxygen vacancies are both positively charged—counter-diffusion of both protons and oxygen vacancies is necessary. Since oxygen vacancies are annihilated at the surface where the partial pressure of steam is high and created at the surface where the steam partial pressure is low, the concentration gradient in oxygen vacancies will be opposite of the steam concentration gradient. Any steam appearing on the surface of the anode by the reverse of reaction (1.3) will be consumed in the reforming and shift reactions (1.1) and (1.2). If current is flowing through the cell, the adsorbed hydrogen will proceed with reaction (1.4). In this case, however, it is not necessary for oxygen ions to migrate since the protons are free to hop between oxygen atoms. A net protonic current will exist if there is an electrochemical potential gradient across the cell and an external load applied.

The kinetics of reactions (1.1) and (1.2) are presumed to be fast at 750 °C, so that the partial pressure of steam at the anode will be very low as long as methane and/or carbon monoxide are present. Steam produced at the cathode by reaction (1.5) will make the steam partial pressure at the cathode much higher than at the anode. Some of the steam appearing at the cathode will undergo reaction (1.3), and return back through the electrolyte to the anode due to the concentration gradient. Protonic conductivity depends only on the concentration and mobility of protonic defects. It is the net flux of protons that provides the Faradaic current of the cell. Steam permeation, on the other hand, depends on correlated motion of both the protons and oxygen ions (and oxygen vacancies). There is, therefore, no net current produced, and the phenomenon occurs independently of the protonic flux, even at open circuit. Steam permeation is thought to be the rate-limiting process, since the activation energy for oxygen vacancy transport is much larger than for protonic transport (~0.7 eV versus 0.45 eV [8,9]).

1.5. Coking

Ambipolar steam permeation makes it possible to apply methane directly to the PCFC anode, without the need for additional external steam injection or partial oxidation of the fuel. Ordinarily in the presence of a nickel catalyst, hydrocarbons will pyrolize to form solid carbon (coking) and/or nickel carbide. Even when ample steam is present in the gas mixture, coking may occur because the reforming reaction requires coincidence of a water molecule arriving at a reaction site near a methane molecule before the methane decomposes. The surface of the PCFC anode, on the other hand, has a monolayer of adsorbed water vapor already present. Rather than requiring adsorption from the gas phase, this water vapor comes from steam permeating through the electrolyte that has diffused through fissures in the nickel anode. Coking cannot occur as long as the flux of water molecules diffusing through the electrolyte keeps up with the rate of hydrocarbon adsorption and decomposition.

2. Experimental

2.1. Electrolyte disc assembly

A disc of 10% yttrium-doped barium cerate, BCY10, protonic ceramic electrolyte was prepared by the traditional powder compaction and sintering method. The disc was ground on each face with a diamond wheel to a thickness of 460 μm. The diameter of the disc was 23 mm.

The cathode surface of the disc was painted with a coating of porous, thick film platinum (Englehard A6101), and sintered for 1 h at 1000 °C. The anode surface of the disc was coated with 1 μm of sputtered nickel using a horizontal magnetron sputtering system. Since nickel is inherently a good mixed electronic/protonic conductor, the triple-phase boundaries required with SOFCs are not required with PCFCs, and can be replaced with 2 two-phase interfaces (gas/electrode and electrode/electrolyte). Such an anode has a large active surface area, low area specific resistance (ASR), and is very catalytically active for reforming methane. Steam permeation is believed to occur along the fissures in the columnar structure of the thin electrode that develop around the nickel grains during coarsening at the elevated operating temperature.

2.2. Cell assembly

The cells were constructed by sandwiching the electrolyte disc assembly (EDA) between the top surface of the lower bipolar disc (anode side) and the bottom side of a second bipolar disc, serving as the cathode, shown in Fig. 3. The stack was held together in the clamping fixture shown unassembled in the figure. The anode disc (shown on the left) had a spiral gas channel milled into the top surface. High purity hydrogen or methane gas was introduced into the cells through the middle stainless steel tube and into the center hole. The fuel flowed through the spiral channel and exited the cell through the hole in the end of the channel and out through the tube on the right. The EDA was placed below the air diffusion screen that served to make electrical contact between the top of the EDA and the cathode bipolar disc, while allowing good air flow for the hydrogen oxidation reaction at the cathode. The air diffusion screen was made from 20 mesh 316 stainless steel, 22.3 mm in diameter. Finally, the cathode disc was placed on top of the air diffusion screen. Low pressure compressed room air was provided to the cathode through the center stainless steel tube from a simple aquarium diaphragm pump. The clamping fixture with four 10–32 machine screws insulated by ceramic sleeves is shown in the middle of Fig. 3. By carefully applying torque to each of the screws it was possible to seal the anode chamber without damaging the delicate EDAs. A small amount of fuel leakage was inevitable, but the lap seal between the EDA and the anode disc provided the necessary compliance for the thermal cycling required for the experiment. The cell assembly was inserted into an alumina ceramic process tube in an electric tube furnace.

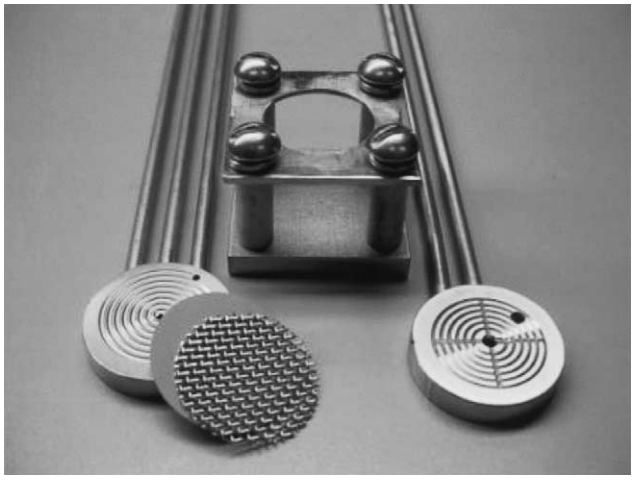

Fig. 3. Anode bipolar disc with spiral gas distribution channel, EDA and air diffusion/current collection screen (left). Cathode bipolar disc inverted (right). Cell clamping fixture (center).

2.3. Electrical measurements

For determining current density, the active surface area of the cell was estimated to be $4.0 \pm 0.2\ \text{cm}^2$. Electrical contacts were made to the anode and cathode bipolar discs using the stainless steel tubes, in a four-wire configuration. The cell voltage and current were measured with a programmable dc electronic load manufactured by Chroma (model 63103 with a model 6312 load module). This instrument was controlled over a general purpose interface bus (GPIB) from a LabView program running on a desk-top computer. With this experimental set-up, it was possible to automatically control furnace temperature and obtain voltage versus current data for the device under test, as required.

Under computer control, a series of current versus voltage characteristic curves was obtained between 600 and 800 and back to 600 °C, in 10 °C steps. The increasing and decreasing temperature scans were repeated continuously throughout the duration of the test. The cell was initially operated for about 100 h on hydrogen (seven complete temperature cycles at 16.5 h per cycle), then switched over to pure methane for three cycles. The slope of each *I–V* curve between 10 and 20 mA/cm^2 was determined. This slope gives the effective cell area specific resistance. After the first complete temperature cycle on methane, there was a steady rise in cell ASR.

Upon disassembly of the cell at the completion of the experiment, no evidence of coking was observed. The EDA was not cracked, and it showed no signs of corrosion (either in the ceramic or the electrodes). The rise in cell ASR during the course of operation on methane was believed to be due to evaporation of nickel from the anode in the high current flux density regions, where contact was made to the anode disc.

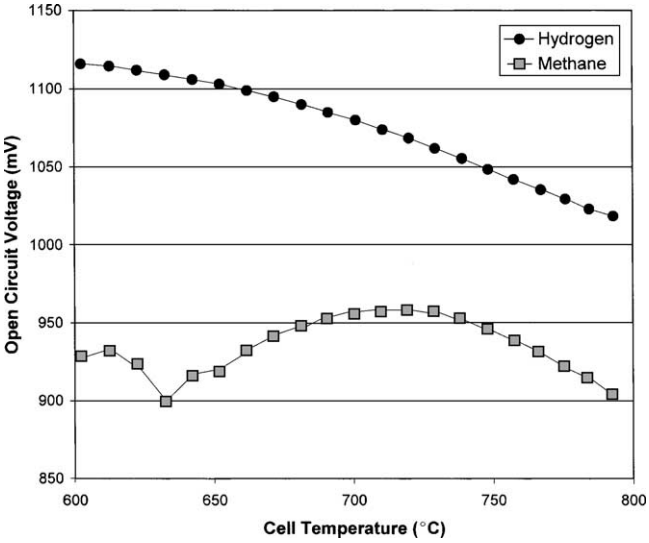

Fig. 4. Open circuit voltage vs. temperature for hydrogen (upper curve) and methane (lower curve). Descending temperatures from 800 to 600 °C in 10 °C decrements.

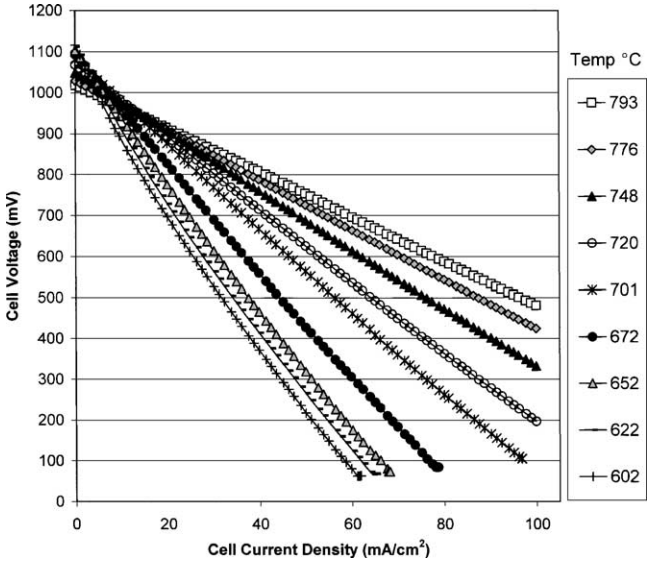

Fig. 5. Hydrogen/air PCFC *I–V* curves for 793–602 °C.

3. Results

3.1. Open circuit voltage

A comparison of the open circuit voltages of the cell during the final (seventh) decreasing temperature scan on hydrogen with the subsequent decreasing scan in methane is shown in Fig. 4. The V_{oc} of the hydrogen cell is very close to the theoretical value at 600 °C, but drops by about 100 mV by 800 °C. This characteristic drop in V_{oc} has often been misinterpreted as evidence for the onset of electronic conductivity, with a corresponding drop in ionic transference number. In a hydrogen cell, steam that permeates to the anode dilutes the hydrogen, lowering its fugacity. The steam permeation flux increases with temperature, so it is expected that the cell potential will drop. The extent of the effect depends on the hydrogen flow rate through the anode chamber and the residence time of adsorbed water vapor on the surface of the anode.

The V_{oc} of the cell on methane shows a complex behavior, with a dip at 630 °C and a new maximum at about 720 °C. The steam permeation and water shift reactions have different equilibrium constants and different reaction kinetics on nickel catalyst. The lower temperature maximum is believed to be due to optimization of the water shift reaction, and the higher temperature maximum is believed to be due to optimal steam reforming. Only at temperatures above about 750 °C does the V_{oc} decline significantly. Whether this is due to electronic conductivity or other mechanisms is unclear at this time.

3.2. I–V characteristic curves

Selected *I–V* characteristic curves (about every 25 °C) for the cells operating on hydrogen and methane are shown in Figs. 5 and 6. It may be observed that the current densities at a fixed voltage are higher with hydrogen than with methane. This is because the methane/air cell has a lower V_{oc} due to the smaller ΔG of the reaction compared with the hydrogen/air reaction. It may also be seen that all *I–V* curves in the hydrogen/air cell are nearly perfectly straight at all temperatures, whereas some of the curves exhibit kinks in the methane/air cell at high current densities. This is believed to be a result of concentration polarization effects in the methane cell, caused by sluggish reaction kinetics at the anode. However, in the operating region of commercial interest (above 600 mV) the curves are all nearly straight at temperatures above about 650 °C. Finally, it is observed

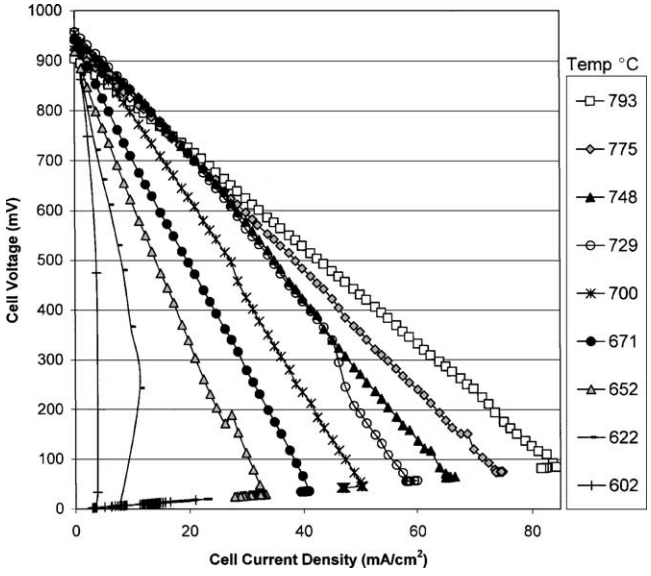

Fig. 6. Methane/air PCFC *I–V* curves for 793–602 °C.

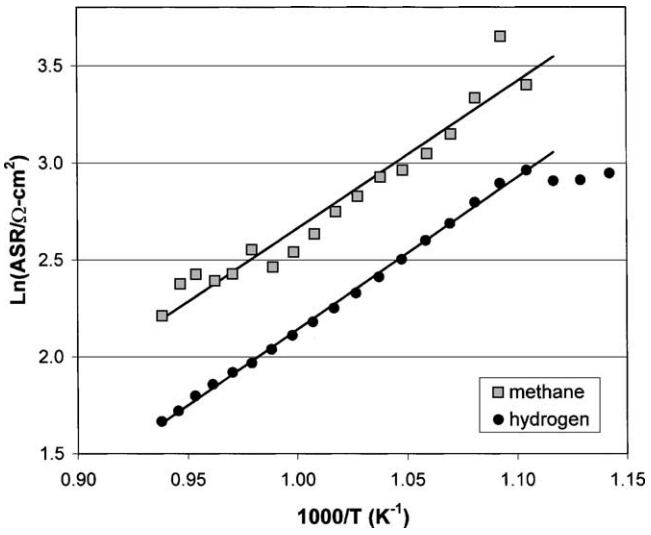

Fig. 7. The ln(ASR) vs. 1000/T obtained at 15 mA/cm^2. Upper curve is for methane and lower curve is for hydrogen.

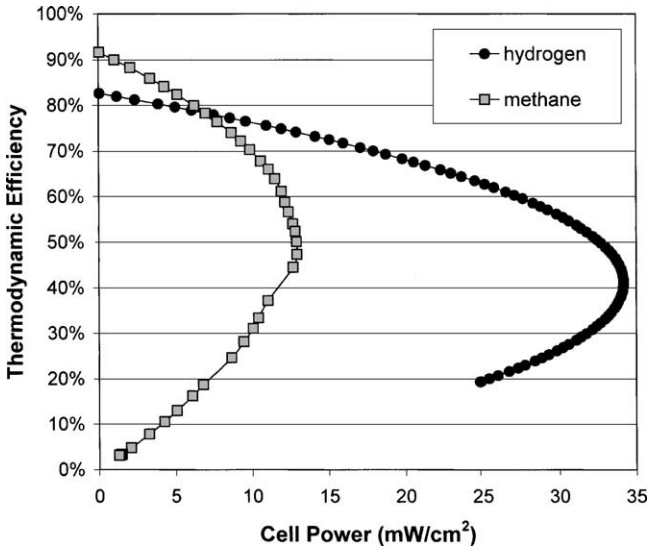

Fig. 8. Thermodynamic efficiency vs. power density for PCFC on hydrogen and methane at 1000 K.

that the current density drops off much more rapidly below 650 °C for the methane cell than for the hydrogen cell. As previously noted, the reforming reaction is favored at a higher temperature than the water shift reaction. Since a methane molecule must undergo the reforming reaction before the water shift reaction can proceed, it is apparent that below about 650 °C the cell becomes rate-limited by the kinetics of reforming. In order to improve the cell performance at lower temperatures, a more catalytically active anode surface than pure, sputtered nickel is needed.

3.3. Area specific resistance

The data of Figs. 5 and 6 are of most use when presented as a plot of the logarithm of the slopes at constant current (15 mA/cm^2) versus reciprocal temperature, as shown in Fig. 7. In the figure, the data for each fuel were fit to a straight line between 650 and 800 °C. It may be observed that, although the curves are offset, due to the different ΔG values for the two reactions, the slopes are nearly identical. This is a rather surprising result since it means that the rate-limiting mechanism is the same whether the fuel is hydrogen or methane. The activation energy for the cell on hydrogen was 0.67 ± 0.01 eV and for the cell on methane was 0.65 ± 0.04 eV. These values are too high to be due to protonic transport, and too low to be due to oxygen vacancy transport. Although an activation barrier due to the electrode/electrolyte interface cannot be ruled out, the intermediate value between pure protonic and pure oxygen ion diffusion suggests there is correlated motion of both species by ambipolar diffusion. It is reasonable that a cell operating on methane would be rate-limited by ambipolar steam permeation, but it is not clear why the cell operating on hydrogen is apparently determined by the same mechanism.

3.4. Thermodynamic efficiency

Finally, it is possible to estimate the thermodynamic efficiency of the PCFC operating on both fuels as a function of output power density. Neglecting the correction for gases not being at standard pressure, ΔH_c for complete oxidation of hydrogen and methane at 1000 K is −193 and −802 kJ/mol, respectively. The thermodynamic efficiency is calculated as

$$\eta_t = \frac{nFE}{\Delta H_c} \tag{3.1}$$

where n is the number of electrons transferred ($n = 2$ for hydrogen and $n = 8$ for methane), F the Faraday's constant and E the cell voltage.

A plot of thermodynamic efficiency versus power density for both fuels is shown in Fig. 8. It may be observed that the cell operating on hydrogen had a much higher maximum power density (34 mW/cm^2 versus 13 mW/cm^2), but at 80% thermodynamic efficiency, the power density on either fuel was about the same (6 mW/cm^2). This is because the intrinsic efficiency of a methane cell at 1000 K is greater than that of a hydrogen cell. Such high values of thermodynamic efficiency would not be possible with externally reformed methane, internally reformed methane with injected steam, or methane subjected to partial oxidation, because of the decrease in fuel fugacity that ensues.

4. Summary and conclusions

The current densities obtained with this cell are much too small, by a factor of 50–100, to be commercially viable. It is expected that reduced electrolyte thickness, improved bulk conductivity, and optimized electrodes will make it possible

to improve current density, in much the same way as has been done with SOFCs.

Direct steam permeation reforming of "dry" methane, without coking, has been demonstrated for extended periods in a PCFC for the first time. A cell with high thermodynamic efficiency and stable operation has been described. Experimental determination of fuel utilization requires careful analysis of exhaust gas as a function of load and temperature conditions. This data will be presented in a subsequent paper.

References

[1] Energy Prices and Taxes—Quarterly Statistics, Energy Information Agency, 2001 (http://www.eia.doe.gov.emeu/international/ngasprih.html and http://www.eia.doe.gov.emeu/international/elecprih.html).

[2] A. Demin, P. Tsiakaras, Thermodynamic analysis of a hydrogen fed solid oxide fuel cell based on a proton conductor, Int. J. Hydrogen Energy 26 (2001) 1103–1108.

[3] R.J. Gorte, H. Kim, J.M. Vohs, Novel SOFC anodes for the direct electrochemical oxidation of hydrocarbon, J. Power Sources 106 (2002) 10–15.

[4] H. Raak, R. Diethelm, S. Riggenbach, The Sulzer Hexis story: from demonstrators to commercial products, in: Proceedings of the Fifth European SOFC Forum, vol. 1, 2002, pp. 425–432.

[5] G. Ma, T. Shimura, H. Iwahara, Simultaneous doping with La^{3+} and Y^{3+} for Ba^{2+}- and Ce^{4+}-sites in $BaCeO_3$ and ionic conduction, Solid State Ionics 120 (1999) 51–60.

[6] M.E. Bertolo-Pardo, et al., Study of proton transport in $BaCe_{0.9}Y_{0.1}O_{2.95}$ and $SrCe_{0.95}Yb_{0.05}O_{2.95}$, in: Proceedings of the 11th International Conference on Solid State Protonic Conductors, PB3, 27–30 August 2002.

[7] G. Ma, D. Jia, L. Qui, Performance of solid oxide fuel cell using $BaCe_{0.9}Y_{0.1}O_{3-\alpha}$ as solid electrolyte, Acta Chim. Sin. 58–61 (2000) 1340–1344.

[8] K.D. Kreuer, Th. Dippel, Yu.M. Baikov, J. Maier, Water solubility, proton and oxygen diffusion in acceptor doped $BaCeO_3$: a single crystal analysis, Solid State Ionics 86–88 (1996) 613–620.

[9] K.D. Kreuer, E. Schönherr, J. Maier, Proton and oxygen diffusion in $BaCeO_3$ based compounds: a combined thermal gravimetric analysis and conductivity study, Solid State Ionics 70–71 (1994) 278–284.